Available online at www.sciencedirect.com
SCIENCE DIRECT®
International Journal of Mass Spectrometry 225 (2003) 261–270
International Journal of Mass Spectrometry
www.elsevier.com/locate/ijms

Near-threshold photoionization spectroscopy of the mono-terpenes limonene and carvone

Gustavo A. Garcia[a,b], Laurent Nahon[b,c], Ivan Powis[a,*]

[a] *School of Chemistry, University of Nottingham, Nottingham NG7 2RD, UK*
[b] *LURE, Bât. 209d, Université de Paris-Sud, 91898 Orsay Cedex, France*
[c] *CEA/DRECAM/SPAM and LFP, Bât. 522, CE de Saclay, 91191 Gif sur Yvette Cedex, France*

Received 11 September 2002; accepted 6 January 2003

Abstract

The photoionization of two representative mono-terpenes (R-limonene and R-carvone) has been investigated using low energy synchrotron radiation in the region from the threshold for ionization of these molecules up to 11 eV. Data from threshold photoelectron spectra are interpreted with the aid of Outer Valence Green's Function (OVGF) calculations to identify the character of the outermost orbitals and improved ionization potentials are deduced.

Fragmentation of the parent ions is studied using threshold photoelectron-photoion coincidence (TPEPICO) time-of-flight (TOF) mass spectrometry and breakdown diagrams identifying the major products in this near-threshold region are presented.

Keywords: Near-threshold; Breakdown; Fragmentation; Photoelectron spectroscopy; Ionization energy

1. Introduction

The terpenes are naturally occurring bio-molecules traditionally regarded as being built up from a number of isoprene [CH_2=C(CH_3)–CH=CH_2] base units, though they also may incorporate additional functional groups. Terpenes are found in plants and are significant components of the extracted essential oils. As such they have found important uses in the flavour and fragrance industry. They may also play important roles in the ecological chemistry of plants involving defence against insects and pathogens and so it is no surprise that others are of interest for pharmaceutical applications. Terpenes will also be emitted into the atmosphere by plants, where they are implicated in aerosol and smog formation. There has also been speculation on the consequences of their reaction with atmospheric ozone on the tropospheric ozone layer.

Overall it can be seen that the terpenes constitute a class of organic compounds of major ecological and industrial importance. The two representative molecules selected for study in this paper are well known in this context, particularly for their distinctive odour characteristics. The monocyclic mono-terpene (i.e., composed of two isoprene units) limonene is the most widespread terpene, found in well over 300 plants, and its two enantiomeric forms (R-(+), S-(−)) are associated with orange/citrus and pine smells, respectively. Likewise R-(−) carvone is used as a flavour enhancer for its spearmint odour, whereas the

* Corresponding author. Tel.: +44-115-951-3467; fax: +44-115-951-3562.
E-mail address: ivan.powis@nottingham.ac.uk (I. Powis).

1387-3806/03/$ – see front matter
doi:10.1016/S1387-3806(03)00004-6

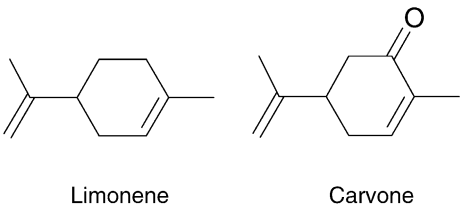

Fig. 1. Structural forms of the title compounds.

S-(+) enantiomer has a smell resembling caraway. S-(+) carvone and R-(+) limonene have more recently received attention for their anticarcinogenic properties [1,2]. The structures of these two molecules are shown in Fig. 1.

Given the importance of these molecules there is potential interest in understanding, and perhaps then exploiting, their mass spectra obtained under "soft" photoionization conditions. Yet to our knowledge, while the 70 eV electron impact mass spectra are of course known, there is only sparse knowledge of the low energy fragmentation channels and their appearance energies that can be gleaned from old electron impact studies on limonene [3] and carvone [4]. Likewise there are no previous published ultraviolet photoelectron spectroscopy (PES) studies of carvone, and only a thumbnail overview of the limonene PES (lacking an energy scale) [5]. Consequently, for both carvone and limonene the only data on the molecular ionization potential comes from the earlier electron impact studies [3,4] with unspecified uncertainties in each case.

In the present paper we make use of tuneable synchrotron radiation and a supersonic molecular beam source of the title molecules to record their time-of-flight (TOF) mass spectra as a function of photon energy in the range from 8 to 11 eV. We also report and examine threshold photoelectron spectra (TPES) for carvone and limonene, which allows us to comment on the stability of the low lying ionic states of these molecules.

2. Experimental

Experiments were performed on the SU5 low energy beamline at the Super-ACO storage ring (LURE, France) using the SAPHIRS molecular beam spectrometer [6]. This is an undulator beamline providing variable polarization in the 5–40 eV photon energy range [7]. The 6.65 m Eagle off-plane normal incidence monochromator was used with 2400 L/mm grating blazed at 900 Å. The entrance and exit slits were set to obtain a typical photon bandwidth ∼3–5 meV. The polarization vector of the light was set parallel to the TOF axis (vide infra) in all the measurements presented here, though checks were also performed with circularly polarized light to look for any obvious chiral effects: none were noted. The photon flux was recorded during each experiment using a gold wire grid and was used to normalize the intensity of the photoelectron spectra. The beamline is also equipped with a gas harmonic filter [8] which, used with Ar, effectively removes second- and higher-order radiation from the delivered <15.7 eV photon beam with an attenuation factor $>10^5$.

The low vapour pressure samples were admitted into the spectrometer as a skimmed, continuous molecular beam seeded in Ar. The stainless steel supersonic nozzle assembly consisted of a small sample reservoir situated immediately below and behind a second chamber containing the pinhole nozzle, and separated from it by a 15 μ sintered steel filter. Two separate, closely regulated heaters heated the lower reservoir section and the top nozzle chamber. This allowed a temperature gradient to be created. The upper nozzle chamber containing the pinhole was maintained at a slighter higher temperature, both during operation and during the heat up/cool down cycles, in order to eliminate possible sample condensation and consequent clogging of the small diameter pinhole. An external copper shroud surrounding the pinhole and upper chamber was used to help achieve more uniform temperature distribution across this region. Copper tubing carrying cooling water surrounded the lower reservoir chamber—this then also allowed cooling when required to maintain the temperature gradient. In operation a stream of argon enters the lower chamber and sweeps sample vapour across the sintered filter. The mixture then expands through the nozzle into an expansion chamber. The beam is then

Table 1
Molecular beam expansion conditions used for the two sample molecules

	Nozzle diameter (μm)	Ar backing pressure (bar)	Expansion chamber pressure ($\times 10^{-4}$, mbar)	Temperature (°C)	
				Reservoir	Nozzle
R-(+) limonene	75	1.3	1	110	115
R-(−) carvone	100	0.4	7	90	120

skimmed by a 1 mm diameter skimmer and enters the main spectrometer chamber where the pressure remained $\approx 10^{-6}$ mbar during all experiments.

Commercial samples of limonene and carvone enantiomers were obtained from Aldrich and used without further purification. The conditions used to create the molecular beams are summarized in Table 1. In addition to the usual advantages, the use of a well collimated sample beam proved to be very effective in preventing any condensation of these low vapour pressure samples on the electrodes of the ion–electron spectrometer, and thus, avoided any consequent degradation of performance with time.

Electrons and ions are produced at the intersection of the molecular and photon beams and are then accelerated in opposite directions into a double TOF spectrometer [6]. The electrons are extracted by a weak constant field and on arrival at the electron detector they can trigger a 81 V pulsed repeller field in the source to expel the ions into a second accelerating region and thence into a drift region, in a conventional Wiley–Maclaren arrangement [9]. Ions are detected on a microchannel plate detector. The electron arrival also serves as a reference start pulse to measure the ion flight time. With this timing arrangement and a 10 K supersonic beam source we have demonstrated an ion mass resolving power better than 150 at mass 150 amu [10].

The S-ACO storage ring operates in either 24-bunch mode, giving light pulses with a 10 ns period or in 2-bunch mode where the pulses are spaced by 120 ns. In the latter case, we are able to measure the electron flight times with respect to the S-ACO pulse providing they are less than 120 ns inter-pulse gap. Hence, electron energies and especially zero kinetic energy threshold electrons can be identified by TOF techniques and TPES can be obtained. The electron resolution in these cases was set to 15 meV (measured on the Ar $^2P_{3/2}$ line) before recording TPES spectra and was rechecked afterwards to ensure there was no long term loss of resolution resulting from sample re-condensation on the spectrometer itself.

TOF ion mass spectra were recorded in coincidence mode using the 24-bunch operation of Super-ACO. Here we rely on the low transmission of energetic electrons possessing more than a few millielectron volts (meV) through the discriminating apertures of the electron TOF assembly to preferentially detect near-threshold electrons (steradiancy analysis). Such electrons will be detected more efficiently, although we will still get some residual contribution from energetic "hot" electrons, with the energetic tail extending up to a few 100 meV. Recording the ion mass spectra in coincidence with these steradiancy analyzed threshold electrons allows us to look at ionic fragmentation of energy and/or state-selected molecular parent ions since the ionization energy is then fixed (to within the resolution of our electron steradiancy analysis) as the selected photon energy. Breakdown diagrams derived from our coincidence mass spectra, therefore, demonstrate the ionization energy-dependent fragmentation and contrast with the integral nature of curves measured purely as a function of photon energy.

3. Results and discussion

3.1. Limonene

The TPES of R-(+) limonene is shown in Fig. 2, and the extracted experimental peak values are listed in Table 2. This measurement was made using the

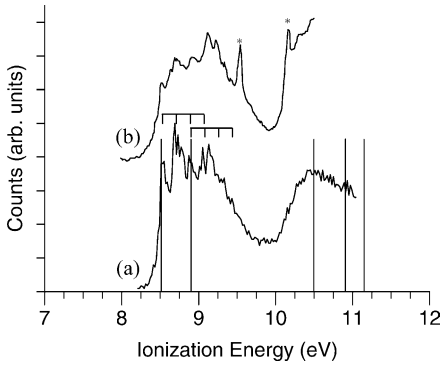

Fig. 2. Limonene photoelectron spectrum. (a) TPES, this work. (b) PES redrawn from [5]. This latter includes two CH_3I calibrant peaks marked (∗). The vibrational progressions calculated using the ring C=C stretching frequency of the neutral limonene are shown on the top of (a) and calculated ROVGF/cc-pVDZ//B3LYP/6-31G** ionization energies are indicated with vertical bars drawn from the abscissa.

2-bunch operating mode of S-ACO, and hence we were able to select the genuine threshold electrons from their recorded TOF relative to the S-ACO light pulse. As mentioned earlier, the only other PES that can be found in the literature was taken by Brint et al. [5], and is redrawn in Fig. 2 for comparison. Rather surprisingly, no energy scale appears in the original PES from these authors, although they added CH_3I calibrant which gives two identifiable peaks at 9.54 and 10.16 eV. We have attempted to derive an energy scale from these two values but note there is some residual uncertainty in this calibration. The two peaks around 9.1 eV are somehow displaced with respect to our results but this may indicate the limitations of the calibration we were forced to adopt for Brint's PES.

The GAUSSIAN 98 package [11] has been used to perform ab initio calculations in order to get some insight into the electronic structure. To calculate the geometry of the ground state, we chose to carry out the optimization by applying density functional theory using the B3LYP functional [12,13] with a 6-31G** basis set. This method is proven to be both computationally cheap and relatively accurate for larger molecules. The optimized geometry was then employed to compute the vertical ionization energies (IEs) of the different molecular orbitals using the Outer Valence Green's Function (OVGF) method [14,15] with a cc-pVDZ basis set. The vertical IEs calculated in this way are plotted in Fig. 2 as a stick diagram, and the values listed in Table 2.

The OVGF calculations identify only two molecular states in the lower energy band region 8.5–9.5 eV; these correspond to ionization of the two π orbitals in the molecule. The HOMO orbital of limonene is calculated to be the π bonding orbital inside the ring while the next orbital in energy relates to the double bond in the isobutenyl. The prominent additional experimental peak located at ∼8.73 eV could be due to a vibrational excitation localized at the molecular orbital being ionized. The vibrational frequencies for inside and outside double bonds in the neutral limonene are 1450 and 1640 cm^{-1}, respectively [16]. The estimated energies for vibrational transitions up to $\nu^+ = 3$ are plotted in Fig. 2 assuming that ionization from

Table 2
Experimental and calculated ionization energies for limonene

Experimental feature	I_{vert} (eV)	I_{vert} (eV)[a]	Calculated (eV)[b]	Suggested assignment
1	8.55	8.54	8.51	Ring π $\nu_{stretch} = 0$
2	8.69	8.71		Ring π $\nu_{stretch} = 1$
3	8.87	8.92	8.90	acyclic π (or ring π $\nu_{stretch} = 2$)
4	9.05	9.08		See text
5	9.13	9.23		See text
			10.49	Ring σ
			10.91	Ring & CH_2–C–CH_3 σ
			11.15	Ring σ

[a] Data extracted from [5].
[b] GAUSSIAN 98 ROVGF/cc-pVDZ//B3LYP/6-31G** calculations, this work.

the HOMO orbital excites the inside C=C stretching mode with a frequency similar to that of the neutral. We can then see that the 8.73 eV peak could well be explained as the $\nu^+ = 1$ vibrational excitation.

The second calculated ionization is predicted at 8.9 eV and can be identified with the third observed feature in the spectrum. In the region ∼9.1 eV there are further features not predicted by the OVGF method which, following the above reasoning, may be due to a vibrational progression. It is not clear from the spectra if there are two peaks in that region or just a broad one and another experiment performed with better statistics and resolution would be needed before we make a more confident assignment. But it is informative to compare this with the PES of related molecules like 1-butene, 2,3-dimethyl—which has an acyclic double bond as is the case in limonene. The evaluated IE for this π system is 9.07 eV [16]. This value should be very close to the second IE of limonene. Consequently, a possible alternative assignment would place the third feature (8.9 eV) as a further member of the vibrational progression built on the HOMO ionization, with the ∼9.1 eV feature(s) corresponding to the adiabatic ionization of the second acyclic π orbital.

The next calculated IEs lie at 10.5 eV and above, and it can be seen from Fig. 2 that the first of these does indeed coincide with the maximum of a broad band in the experimental spectrum. A small shoulder which also coincides with the fourth calculated peak which is identified to be a delocalized σ orbital extending over the full molecule.

Mass spectra of limonene were recorded in coincidence with steradiancy analyzed threshold electrons over a range of photon energies. The coincidence detection means that the internal energy deposited in the parent ion is essentially that of the photon subject only to the limitations of steradiancy analysis which does not completely reject all the hot electrons. These threshold photoelectron-photoion coincidence (TPEPICO) TOF mass spectra are shown in Fig. 3, and the breakdown diagram derived from these data is presented in Fig. 4.

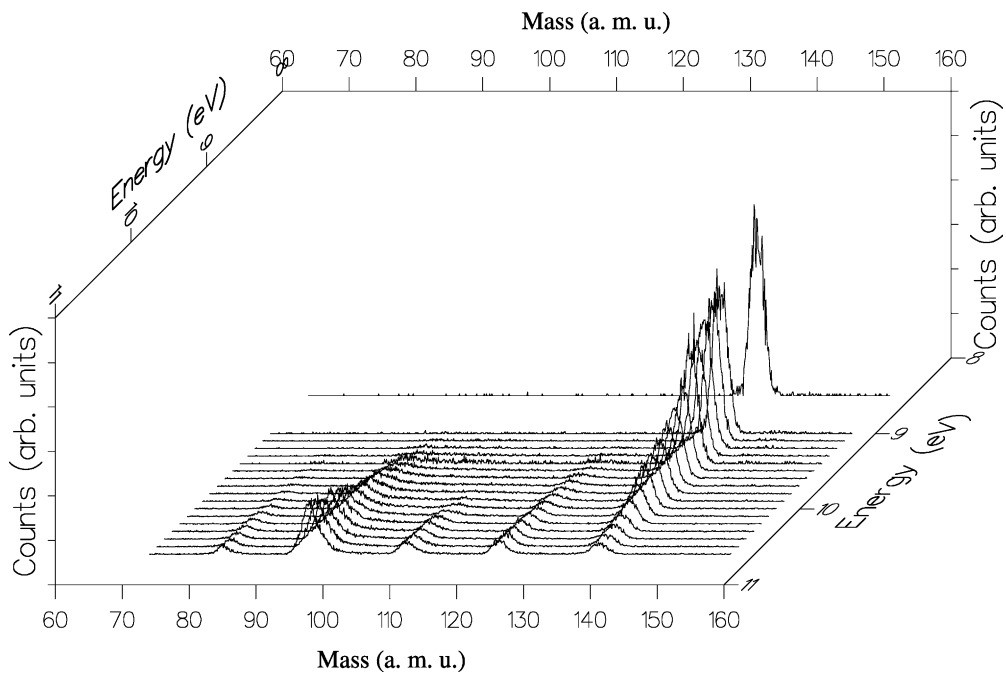

Fig. 3. Limonene TPEPICO ion TOF spectra (recorded in coincidence with steradiancy analyzed threshold electrons) as a function of photon energy.

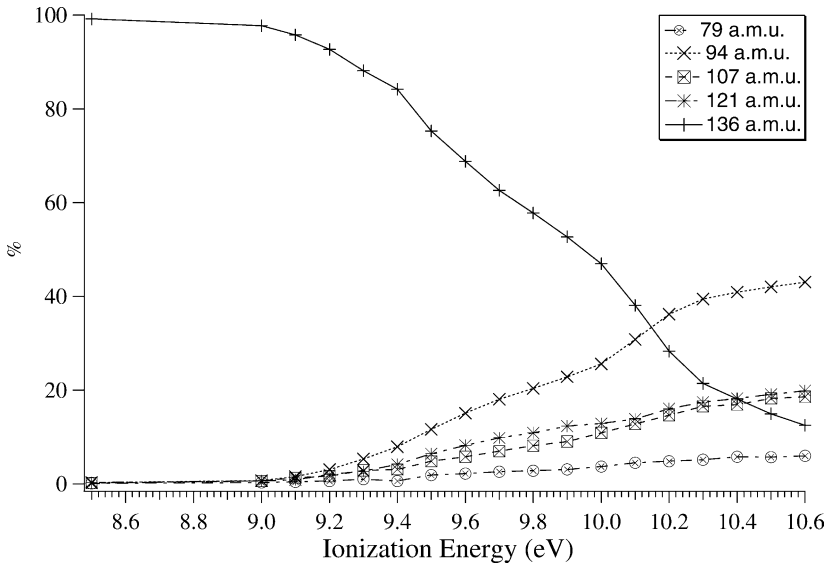

Fig. 4. Limonene ion breakdown diagram derived from data of Fig. 3.

The most intense fragment in this range is C_7H_{10} (94 amu) with an onset around 9 eV. In fact, this appearance energy is common to essentially all the observed fragments coming from the parent limonene (136 amu), which suggests that it may originate from some dynamic barrier rather than reflecting the true energetic thresholds for individual decay channels. Partial support for the existence of a dynamic bottleneck may be found in the observed asymmetric tailing to long flight time of the 94 amu fragment ion peak. This is likely evidence of metastability (slow fragmentation) and is evident even at 10.6 eV, well above the appearance energy.

From the TPES of Fig. 2 and the above discussion we see that the vertical IE for the ionic ground state is 8.55 eV which falls below the fragmentation onset. However, the vertical IE of the second ionic state is either 8.92 or 9.08 eV, which coincides with the onset of observed fragmentation. Hence, we infer that that while the Franck–Condon accessible region of the ground electronic surface is evidently stable, the dissociation channels open with excitation via the first excited ionic state. One may speculate on the possibility that there exists some non-adiabatic seam leading from the excited surface and that this creates a dynamic bottleneck common to all the channels. Looking at the breakdown diagram of Fig. 4 there is some further evidence for a change in slope at ∼10 eV, which corresponds to the onset of the σ bond orbital ionization in the TPES.

The present results may be compared with earlier electron impact ionization measurements [3]. The quoted parent ion appearance potential of 8.3±0.15 eV is in reasonable agreement with the present results, as is the quoted 8.9 ± 0.15 eV appearance energy for the $C_9H_{13}^+$ fragment (121 amu). But these authors do not identify the other fragmentation channels which we see opening up around 9 eV ($C_6H_7^+$, $C_7H_{10}^+$, and $C_8H_{11}^+$, respectively, 79, 94, 107 amu). Of particular concern for this earlier study was the nature of the fragmentation channel producing $C_5H_8^+$ (68 amu). This was inferred to be an isoprene unit resulting from a retro Diels–Alder reaction having a significant activation energy. Thus, while this is a dominant fragment in 70 eV electron impact mass spectrum, it was not observed in lower energy collision-induced ion dissociation spectra. Our present results confirm that this channel is not accessible at low energies, at

least up to 10.5 eV, in accord with its electron impact appearance energy of 11.6 ± 0.15 eV [3].

4. Carvone

The TPES of carvone is shown in Fig. 5 which also includes for comparison the same region taken from two previously unpublished photoelectron spectra of carvone: a He I ($h\nu = 21.2$ eV) PES (Cheetham and Seddon, personal communication) and a higher photon energy $h\nu = 95$ eV PES recorded at the BESSY II synchrotron (Rennie and Garcia, unpublished data). It can immediately be seen that the previously accepted ionization energy of 9.77 eV [4,16], obtained by an electron impact ionization method, is significantly too high, and that a revised estimate should be 8.7 ± 0.05 eV.

As was the case for limonene, above, we performed OVGF/CC-pVDZ calculations to estimate vertical ionization energies, working with the B3LYP/6-31G** optimized geometry of carvone. Three ionizations are predicted to fall in the 8–10 eV range from orbitals formed from the oxygen lone pair and the two C=C π systems. There is, however, a strong mixing of the two localized π orbital descriptions, making the descriptions rather approximate. Simply applying Koopman's theorem to the orbital eigenvalues yields ionization energies with the order acyclic (+ ring) π < ring (+ acyclic) π < n_O. However, the more sophisticated OVGF treatment, which incorporates a treatment for electron correlation energy, places the O lone pair orbital's IE between those of the two π bonds, as shown in Table 3.

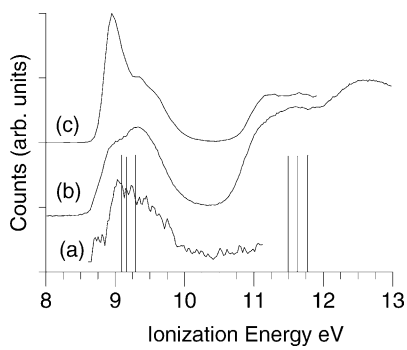

Fig. 5. Carvone photoelectron spectrum. (a) TPES, this work. (b) $h\nu = 21.2$ eV He I PES (Cheetham and Seddon, personal communication). (c) $h\nu = 95$ eV PES (Rennie and Garcia, unpublished data). The calculated ROVGF/cc-pVDZ//B3LYP/6-31G** ionization energies are indicated with vertical bars drawn from the abscissa.

Table 3
Experimental and calculated ionization energies of the lower ionic states of carvone

Feature	I_{vert} (eV)	Calculated (eV)[a]	Assignment
1	8.95	9.16	n_O
2	9.35[b]	9.09	Acyclic (+ ring) π
3	9.35[b]	9.29	Ring (+ acyclic) π
4	11.55	11.49	Ring—C_3 σ bond
		11.62	C=O π
		11.78	Ring σ

[a] ROVGF/cc-pVDZ//B3LYP/6-31G** calculations, this work.
[b] The second and third states are believed to overlap in the experimental spectra and the same peak value is quoted.

Empirical considerations suggest yet another order for these three outermost orbitals. It can be seen that the first band in the photoelectron spectrum has a greater relative intensity in the $h\nu = 95$ eV PES than in either the $h\nu = 21.2$ eV PES or the TPES. Such a relative enhancement, certainly that between the two fixed photon energy PES, would be empirically expected for an orbital with a significant atomic O 2p character [17], suggesting assignment of the HOMO orbital as the carbonyl lone pair. It is further evident that the second and third IEs cannot be experimentally resolved and appear as a single broad feature, peaking at ∼9.3 eV, in all the spectra. It is plausible to suggest assignment of the second experimental band as the two mixed C=C π systems. The re-ordering of these assignments suggested here is shown in Table 3.

At higher binding energies, we find only one broad peak spanning the energies 11–12 eV. According to the OVGF calculations the ionization of the carbonyl C=O π system should appear in this region together with the onset of C–C σ bond ionizations; again with deviations from the simple Koopman's approximation ordering.

In the TPEPICO mass spectrum of carvone (Fig. 6) we were able to detect not just the parent monomer

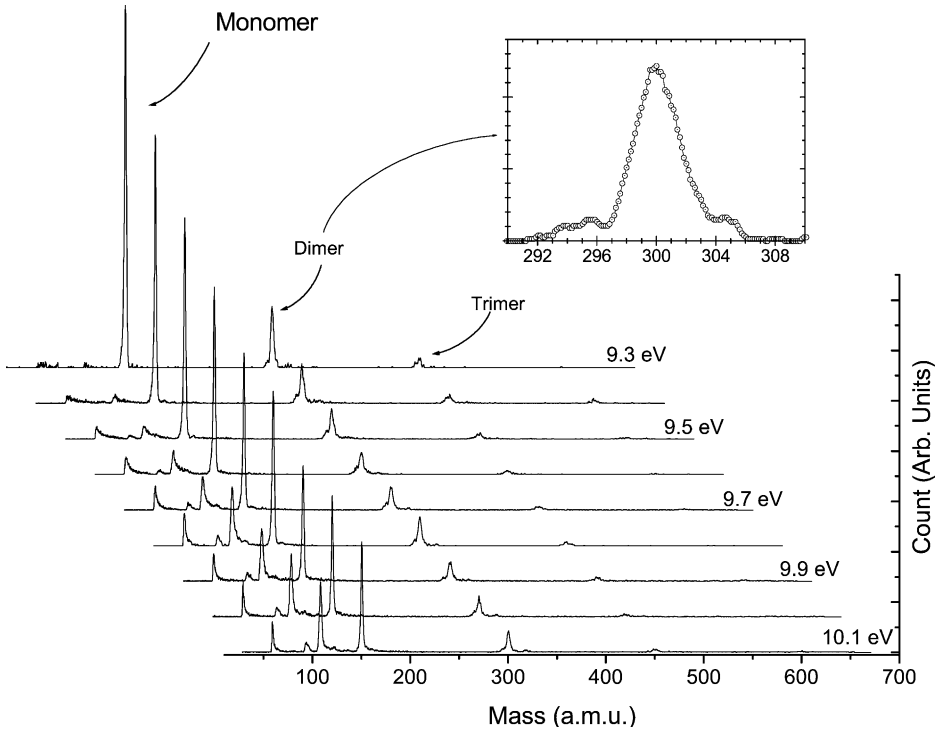

Fig. 6. Carvone TPEPICO ion TOF spectra (recorded in coincidence with steradiancy analyzed threshold electrons) as a function of photon energy in range 9.3–10.1 eV. The inset shows expanded detail of the dimer ion peak (300 amu) at $h\nu = 9.3$ eV.

ion (150 amu) but also the dimer, trimer, and traces of tetramer carvone species. No direct evidence for clustering with the argon carrier gas was observed. The carvone monomer peak has a greater width than was anticipated from an accompanying study using the same apparatus in which the two Br isotopes in CF_3Br were clearly resolved ($\Delta m = 2$) at essentially the same mass (~150 amu) and with an inferred beam temperature of 10 K [10]. Here the carvone peak widths suggest a temperature of ~250 K. This is perhaps surprising in view of clustering observed in the beam, even though although this figure is likely an overestimate as the width also includes a contribution from the unresolved ^{13}C present at natural abundance, and even though some reduction in cooling would be expected in these present studies (due to using a heated nozzle source). Most likely, it is indicative of the formation of some carvone ion by the dissociative photoionization of higher *n*-mer neutrals; the accompanying release of kinetic energy being responsible for broadening the observed ion peak. Similar estimates and inferences may be applied to the dimer ion peak, which additionally has a distinct structure, as can be seen in the inset (Fig. 6). However, the statistics and intensity were not sufficiently good to merit further investigation of this interesting observation.

The principal daughter ion peaks can be seen to display some asymmetry, tailing to high mass. This reduces somewhat with increasing ionization energy, and may be attributable to either some metastability in this near-threshold region, or to unresolved fragments of formula $C_xH_{y,y+1,y+2,\ldots}O^+$. The breakdown diagram (Fig. 7) has been prepared by integrating the asymmetric peaks, which are then identified by the nominal (peak) mass component.

The most intense fragment ion observed is $C_7H_8O^+$ (108 amu). Although, regrettably, we were unable to obtain mass spectra below an ionization energy of

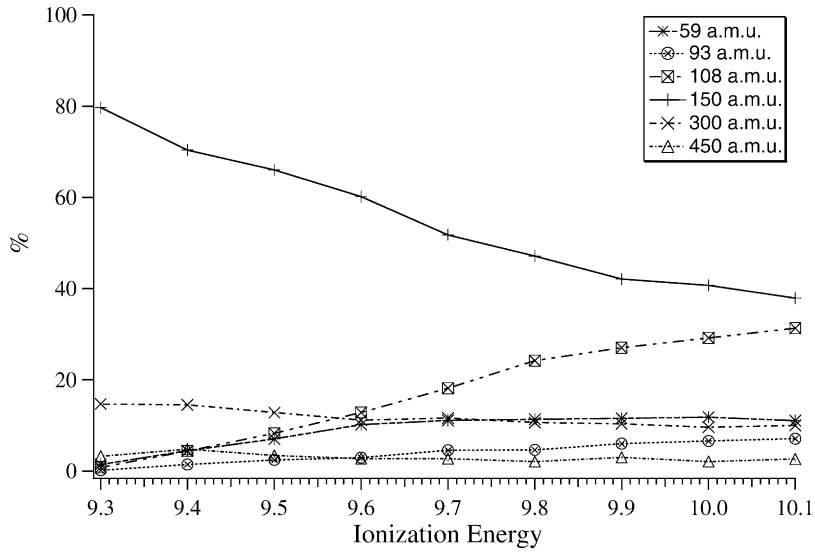

Fig. 7. Carvone ion breakdown diagram derived from data of Fig. 6. The indicated fragment ion masses are nominal (see text).

9.3 eV it seems from the breakdown diagram in Fig. 7 that its appearance potential, and that of the other fragments, will be around 9.3 eV. This falls in the region of the overlapping second/third ionization peaks in the PES. It is plausible to assume that, since the ground ionic state is believed to correspond to the removal of a non-bonding electron from the oxygen atom, there will be little fragmentation from the first ionic state—that is in the region from the adiabatic threshold to ~9.3 eV. Ionization of the C=C π systems, on the other hand, would be expected to be more disruptive of the molecular skeletal bonding and so quite reasonably accounts for the inferred ~9.3 eV fragmentation onset.

Once again, as with limonene, there is no evidence for any retro Diels–Alder type breakdown into constituent isoprene units (C_5H_8 or C_5H_6O).

It is remarkable that, even at the higher photon energies, negligible amounts of daughter ions at masses intermediate between the monomer and the higher *n*-mer are observed. We thus infer that any dissociative photoionization of a carvone moiety within a cluster must lead to a complete rupture of the cluster linkage such that only sub-monomer mass ion fragments result. On the other hand, if at least a proportion of the observed dimer and trimer ion results from dissociative ionization of higher neutral clusters, as discussed before, then one may suppose that a proportion of the excess energy is carried off by the neutral species (and some evidently goes into translational energy). This thus suggests a mechanism for stabilizing the resulting ion. The relative intensity of the *n*-mer cluster species does not fully track that of the monomer, as can be seen also in the breakdown diagram (Fig. 7). While the relative abundance of monomer halves over the photon energy range 9.3–10.1 eV there is a less pronounced drop in abundance of the dimer, and even less for the trimer, and so this tends to support the above suggestion. Nevertheless one might expect, on statistical grounds, that the energy partitioning would leave at least some of the dimer, trimer, etc. ion population with sufficient energy to fragment, so that the complete absence of such fragmentation to intermediate masses remains surprising. Overall then, the dimer, etc. appear to be relatively more stable than the monomer in this near-threshold region, at least with respect to fragmentation within a single carvone entity.

5. Conclusions

In this paper, we have considered photoionization of two representative mono-terpenes in the near-threshold region. The photoelectron spectra can be interpreted to reveal the location and orbital characteristics of the first few electronic states of each ion. Ion fragmentation patterns of state-selected parent ions have then been examined by recording TOF mass spectra in coincidence with steradiancy selected threshold electrons, using tuneable synchrotron radiation to examine an energy range extending up to a few electron volts (eV) above the adiabatic ionization thresholds.

These results establish several new low energy fragmentation channels for each molecule under study, and also suggest that the previous value for the ionization potential of carvone is significantly too high. But of equal importance we find that the ground electronic states are, in each case, relatively stable to fragmentation, providing high yields of the parent ion. In the case of limonene this ground ionic state is formed by ionizing the ring π system; in carvone it is an essentially non-bonding carbonyl oxygen lone pair electron which is removed to form the ground ionic state.

Acknowledgements

We are grateful to the general staff at LURE for operating the Super-ACO storage ring and to B. Pilette for technical help on the SAPHIRS experiment and the SU5 beamline. We thank Prof. E. Seddon for providing the He I PES of carvone. Computational resources on a COMPAQ ES40 multiprocessor cluster (Columbus) at the Rutherford Appleton Laboratory (RAL) were provided by the UK Computational Chemistry Facility.

References

[1] I.A. Hakim, R.B. Harris, C. Ritenbaugh, Nutr. Cancer 37 (2000) 161.
[2] G.Q. Zheng, P.M. Kenney, L.K.T. Lam, Planta Med. 58 (1992) 338.
[3] D. Harris, S. McKinnon, R.K. Boyd, Org. Mass Spectrom. 14 (1979) 265.
[4] G. von Bunau, G. Schade, K. Gollnick, Z. Anal. Chem. 227 (1967) 173.
[5] P. Brint, E. Meshulam, A. Gedanken, Chem. Phys. Lett. 109 (1984) 282.
[6] M. Richard-Viard, A. Delboulbe, M. Vervloet, Chem. Phys. 209 (1996) 159.
[7] L. Nahon, C. Alcaraz, J.L. Marlats, B. Lagarde, F. Polack, R. Thissen, D. Lepère, K. Ito, Rev. Sci. Inst. 72 (2001) 1320.
[8] B. Mercier, M. Compin, C. Prevost, G. Bellec, R. Thissen, O. Dutuit, L. Nahon, J. Vac. Sci. Tech. A 18 (2000) 2533.
[9] W.C. Wiley, I.H. Maclaren, Rev. Sci. Inst. 26 (1955) 1150.
[10] G.A. Garcia, P.M. Guyon, I. Powis, J. Phys. Chem. A 105 (2001) 8296.
[11] M.J. Frisch, G.W. Trucks, H.B. Schlegel, G.E. Scuseria, M.A. Robb, J.R. Cheeseman, V.G. Zakrzewski, J.A. Montgomery, R.E. Stratmann, J.C. Burant, S. Dapprich, J.M. Millam, A.D. Daniels, K.N. Kudin, M.C. Strain, O. Farkas, J. Tomasi, V. Barone, M. Cossi, R. Cammi, B. Mennucci, C. Pomelli, C. Adamo, S. Clifford, J. Ochterski, G.A. Petersson, P.Y. Ayala, Q. Cui, K. Morokuma, D.K. Malick, A.D. Rabuck, K. Raghavachari, J.B. Foresman, J. Cioslowski, J.V. Ortiz, A.G. Baboul, B.B. Stefanov, G. Liu, A. Liashenko, P. Piskorz, I. Komaromi, R. Gomperts, R.L. Martin, D.J. Fox, T. Keith, M.A. Al-Laham, C.Y. Peng, A. Nanayakkara, M. Challacombe, P.M.W. Gill, B.G. Johnson, W. Chen, M.W. Wong, J.L. Andres, C. Gonzalez, M. Head-Gordon, E.S. Replogle, J.A. Pople, GAUSSIAN 98 Revision A.9. Gaussian Inc., Pittsburgh PA.
[12] A.D. Becke, J. Chem. Phys. 98 (1993) 5648.
[13] C.T. Lee, W.T. Yang, R.G. Parr, Phys. Rev. B 37 (1988) 785.
[14] W. von Niessen, J. Schirmer, L.S. Cederbaum, Comp. Phys. Rep. 1 (1984) 57.
[15] V.G. Zakrzewski, O. Dolgounitcheva, J.V. Ortiz, J. Chem. Phys. 105 (1996) 8748.
[16] P.J. Linstrom, W.G. Mallard (Eds.), NIST Chemistry WebBook, NIST Standard Reference Database, 69th ed. National Institute of Standards and Technology, Gaithersburg, MD 20899, 2001. http://webbook.nist.gov.
[17] A. Schweig, W. Thiel, Mol. Phys. 27 (1974) 265.